Surface Science 82 (1979) 177–194

OXYGEN ADSORPTION ON Cu($\bar{1}$10): DETERMINATION OF ATOM POSITIONS WITH LOW ENERGY ION SCATTERING

A.G.J. DE WIT, R.P.N. BRONCKERS and J.M. FLUIT
Fysisch Laboratorium Rijksuniversiteit Utrecht, Utrecht, The Netherlands

Received 2 May 1978; manuscript received in final form 1 September 1978

The position of adsorbed oxygen on Cu($\bar{1}$10) surfaces was determined with Low Energy Ion Scattering (LEIS). The experiments were performed by bombarding the copper surface at small angles of incidence with low energy Ne^+ ions (3–5 keV). Measurements of the Ne^+ ions scattered by adsorbed oxygen showed regular peaks in the azimuthal distribution of the scattered ions due to a shadowing effect. From the symmetry of the azimuthal distributions it follows that the centre of an adsorbed oxygen atom on the Cu($\bar{1}$10) surface lies about 0.6 Å below the midpoint between two neighbouring Cu atoms in a ⟨001⟩ row. A comparison of the azimuthal distributions of Ne^+ ions scattered from clean Cu surfaces and oxygen-covered Cu surfaces showed that hardly any surface reconstruction had occurred in the oxygen-covered surfaces. The applied method seems to be an appropriate one for locating adsorbed atoms because it uses only simple qualitative considerations about azimuthal distributions of scattered ions.

1. Introduction

Various analytical techniques have been used in recent years to investigate adsorbed layers on solid surfaces. The purpose of these investigations is to study the kinetics of adsorption and diffusion processes and to determine the position and binding state of the adsorbed atoms or molecules.

To study adsorption kinetics and binding states, work function measurements, Auger electron spectroscopy (AES), photon electron spectroscopy (ESCA and UPS), thermal desorption techniques, and static secondary ion mass spectrometry (SIMS) have been successfully used [1]. However, it should be realized that a measuring technique can change the adsorption processes. Recently ellipsometry has been combined with AES to study the adsorption kinetics of oxygen on Cu surfaces [2,3]. Low Energy Ion Scattering investigations were performed to study the ion bombardment induced desorption of oxygen on metal surfaces [4] and the adsorption kinetics of oxygen on Cu surfaces [5].

Only very few techniques have been used to determine the position of adsorbed atoms on metal surfaces. Low Energy Electron Diffraction (LEED) experiments have shown regular patterns in oxygen–copper combinations [6–8]. However, it is

not simple to estimate the position of adsorbed atoms with this technique; this can be done only be means of extended calculations. Low energy ion scattering has also been used to estimate the position of an adsorbed oxygen atom on a metal single crystal. Investigations on Ag(110) for example have shown that the oxygen atom on this surface is in a bridge position in a ⟨001⟩ chain on the surface [9]. The position in this chain has been estimated by using an assumed interatomic potential between the noble gas ion and the metal atoms. In the present paper it will be shown that the position of the atomically adsorbed (chemisorbed) oxygen above or below the surface can be determined more directly by using only the symmetry aspects of the resulting low energy ion scattering data. For this determination certain properties of the shadow cone model will be used.

Since the theoretical aspects of shadow cones have been treated extensively by Martynenko [10,11], only those aspects of the shadow cone model will be discussed which are relevant for the structure determination (section 2). The model will be used to interpret the results of the experiments concerning clean and oxygen covered Cu($\bar{1}10$) surfaces (section 4).

2. Angular and energy dependence of ion scattering

2.1. Shadow cone model

Possible projectile trajectories are schematically given in fig. 1 for a binary collision between a projectile (ion) with mass M_1 and a target particle (atom) with mass M_2. Fig. 1a demonstrates the existence of a shadow cone, i.e. an area behind the target atom where no scattered projectiles will be found. The figure shows that when the distribution of particles is homogeneous over the impact parameter an increased intensity of scattered projectiles will occur (at some distance behind the target atom) just outside the edge of the shadow cone. The scattering angle ϑ (fig. 1b) is determined by the impact parameter P according to a function $\vartheta(P)$ [12,13] which also contains the parameters E_0 (the projectile primary energy), M_2/M_1 (the mass ratio) and the assumed spherical-symmetric potential between the colliding particles.

In many cases it is reasonable to suppose that the function $\vartheta(P)$ decreases monotonically from π at $P = 0$ to zero at $P = \infty$. Let S be the distance between the scattered particle and the central axis (in fig. 1b) at a distance L behind the scattering centre; then

$$S = P + L \tan \vartheta \tag{1}$$

in first order approximation (L larger than P and small scattering angles).

Because $\vartheta(P)$ decreases monotonically to zero, dS/dP will be zero for a certain value P_0 of P at fixed L. The corresponding minimum value S_0 defines the width of

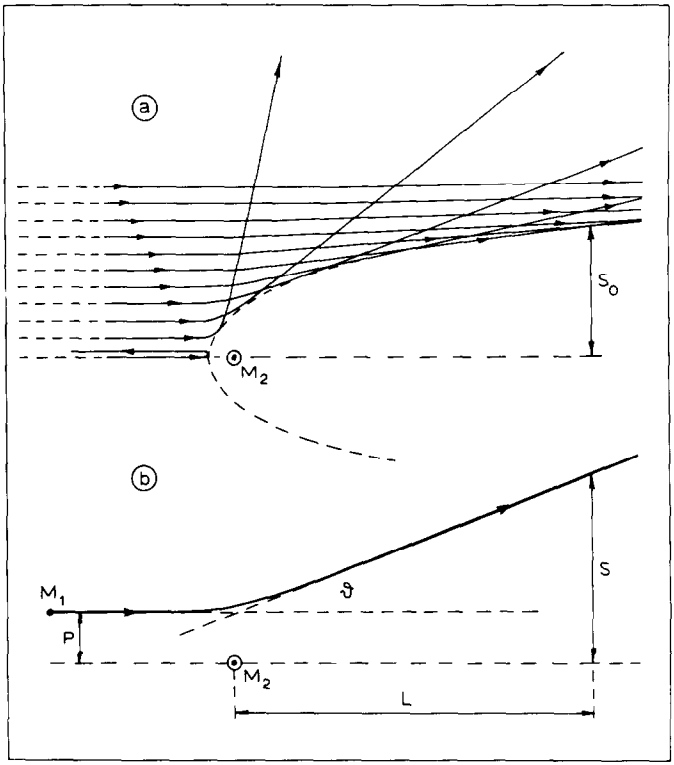

Fig. 1. Possible trajectories of a projectile M_1 scattered by a target particle M_2. In (a) the shadow cone behind M_2 is shown. In (b), S gives the position of the scattered particle for a particle with impact parameter P and scattering angle ϑ, at a distance L behind the scattering centre. (The example shown here is calculated for 5 keV Ne^+ ions on a Cu atom with impact parameters varying between 0.1 and 1.0 Å, using the interaction potential of fig. 2.)

the shadow cone at a distance L behind the scattering centre. Intensity calculations with an inverse square power potential [14] result in an intensity distribution ($F(S)$), as shown in fig. 2. It is generally assumed that this potential is a reasonable approximation for interatomic distances between 0.1 and 1 Å [15,16]. The curve in fig. 2 depends (of course) on the distance L behind the target atom and on the primary energy of the incoming ions.

When a second target particle is situated at (or just outside) the edge of the shadow cone at some distance behind the first target atom the second one will receive an increased flux of projectiles. However, when the second atom is inside the shadow cone a hard collision between the primary particle and the second atom is impossible. In the case of atom rows (as in monocrystals) this means that no hard collision is possible between a projectile and any row atom.

The shadow cone model has already been successfully applied to explain differ-

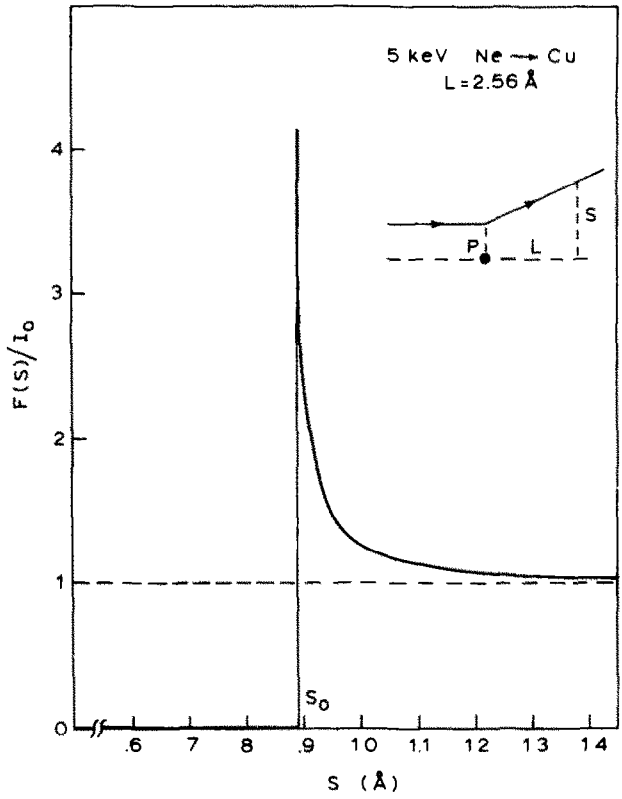

Fig. 2. The calculated relative density of 5 keV Ne particles scattered by a Cu atom at the position (L, S) in the scattering plane (L fixed). (The primary density is indicated by I_0.) The calculations were performed with an inverse square power potential ar^{-2} using parameter a = 132 Å^2 eV.

ent types of ion–surface scattering experiments [17–22]. In the present paper this model is used for the interpretation of the scattering of Ne^+ ions on clean and oxygen-covered Cu(1̄10) single crystal surfaces. An ion beam is directed towards the surface in a direction that permits the detection of double scattering on two neighbouring surface atoms (see fig. 3). More precisely, projectile ions are scattered at the edge of the shadow cone of a target atom and collide with a neighbouring atom. The increased flux of projectiles scattered by the second atom permits the determination of relative atom positions.

2.2. Energy dependence

The experiments were performed by bombarding a Cu(1̄10) surface with noble gas ions (Ne^+). The energy of the ions scattered by specific target atoms in a chosen

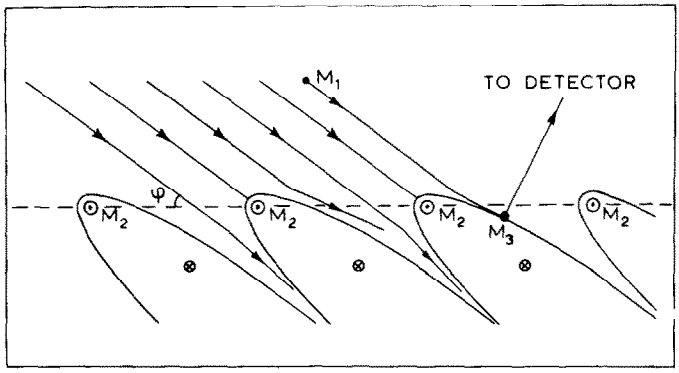

Fig. 3. The shadow cone model applied to a crystal surface. Projectiles (M_1) incident at an elevation angle φ give rise to the shadow cones. An atom (M_3) at the edge of the shadow cone causes a large flux of particles into the detector. The target atoms in the second layer are inside the shadow cone (in this case).

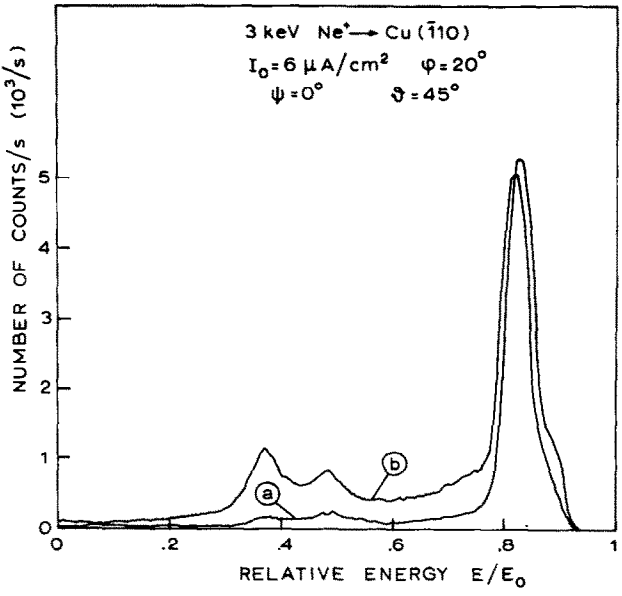

Fig. 4. Measured energy spectra of "reflected" ions for (a) almost clean Cu(1̄10) (10% of the oxygen saturation coverage) and (b) oxygen-covered Cu(1̄10) (60% of saturation coverage). The single scattering peaks of Ne scattered by O and Cu should be found at $E/E_0 = 0.36$ and 0.83 respectively according to formula (2).

scattering angle could be predicted by means of the single scattering model.

In the single scattering model the target atoms are considered to be free atoms. Then the well-know relation between the energy E_1 after scattering and the scattering angle ϑ holds for a collision between a projectile and one target atom. This relation, which follows from the conservation laws for energy and momentum [12], is given by

$$\frac{E_1}{E_0} = \left\{ \frac{1}{1+A} \left[\cos\vartheta \pm (A^2 - \sin^2\vartheta)^{1/2} \right] \right\}^2 \tag{2}$$

(for a target atom initially at rest) where E_0 is the primary projectile energy and $A = M_2/M_1$ is the mass ratio with M_1 the projectile mass and M_2 the target atom mass. When this relation holds, one can measure the scattering that is caused by a specific kind of target atom in a mixed target. For this purpose one has to adjust the selective detector to the projectile energy E_1 which is related to the chosen energy of incidence E_0 and the scattering angle ϑ according to formula (2). This is demonstrated in fig. 4, where energy spectra of scattered (and sputtered) ions for a given projectile energy are shown. The energy spectrum for Ne^+ ions impinging on an oxygen-covered surface shows 3 peaks, which are caused by Ne^+ ions reflected on O atoms ($E_1/E_0 = 0.36$), O^+ ions sputtered from the surface in a single collision process ($E_1/E_0 = 0.49$ for these recoil ions) and Ne^+ ions scattered by Cu atoms ($E_1/E_0 = 0.83$). The high energy shoulder at $E_1/E_0 = 0.9$ is due to multiple scattering from a ⟨110⟩ Cu chain.

3. Experimental

3.1. Introduction

The determination of the chemical composition of a surface becomes considerably easier when large scattering angles are used because it is then simpler to differentiate between different atomic species. Furthermore large elevation angles for the particle directions after scattering are advantageous for the reduction of undesirable blocking and neutralization effects. Therefore in our experiments we used large elevation angles after scattering.

In reality scattering by an atom at a metal surface is not exactly a single collision process. Often, however, the energy of the particles after this type of scattering deviates only slightly from the corresponding energy E_1 of formula (2). Ions scattered by atoms with a specific mass show a shift of only a few per cent compared to formula (2) [24] (cf. fig. 4). Only in special circumstances (for instance very low primary energies and/or small scattering angles) is there a larger shift between experimental and calculated relative energy [23]. This shift is caused by the binding of surface atoms and by the proximity of other surface atoms. In both cases the

secondary energies of scattered ions are higher than with single scattering.

In our experimental circumstances the energy varied for different types of experiments (as shown in section 5), but control measurements showed that the shift was always less than 3% of the primary energy. The maximum shift was found for double scattering in one plane by nearest neighbour atoms for the special case where projectile ions are scattered slightly by first target atoms and are then involved in hard collisions with the second atoms situated at the edge of the shadow cone of the first ones. Calculations confirm this maximum energy shift for the above mentioned double scattering process. This energy shift after scattering is small compared to the experimental energy spread (see fig. 4 and section 5).

Therefore it is possible to study the atomic position of specific atoms on a surface by means of this type of ion scattering experiment, because the detection energy can be determined from the single scattering model and the measured results can be interpreted using the shadow cone model.

3.2. Set-up and handling

The experimental set-up has been described in more detail elsewhere [24]. The main parts of the set-up are a Nier-type ion source (energies 0.1–10 keV, energy spread 1%, angular spread 1°, current 10 nA to 1 μA, spot size 4 mm^2, noble gas ions), a target manipulator (6 degrees of freedom) and a flat-plate electrostatic energy analyzer rotatable in one plane (energy resolution 3.5%, solid space angle 10^{-3} sterad). The background pressure in the target chamber is 10^{-8} to 10^{-9} Torr. From the energy analyzer the analyzed ions are accelerated towards and counted by a Mullard B1407 Channeltron multiplier. The energy analyzer can be rotated in the plane of incidence (defined by the incoming beam direction and the target surface normal) over the angle ϑ (defining the selected scattering angle) from 0° to 145° with respect to the ion beam. The angular resolution $\Delta\vartheta$ is 2–6° depending on the values of the angles φ (defined below) and ϑ. The angular resolution $\Delta\psi$ is 3.5° (ψ defined below).

The experiments were performed on copper single-crystalline targets at room temperature. The targets were prepared by mechanical and electro-lap polishing and were cleaned by ion bombardment (with an ion dose of about 10^{17} ions/cm^2 at an energy of some keV) before each series of measurements. The measurements were performed in the following way. A certain elevation angle of incidence φ (the angle between the direction of the incoming ion beam and the target surface plane) was adjusted by means of the manipulator ($0° \leqslant \varphi \leqslant 140°$). A certain scattering angle ϑ was chosen and the analyzer was adjusted for a certain detection energy to measure a specific scattering process ($Ne^+ \rightarrow O$ or $Ne^+ \rightarrow Cu$). Azimuthal distributions $N(\psi)$ were measured by rotating the crystal around the surface normal. ψ is the angle between the projection of the incoming beam direction on the surface plane and the ⟨110⟩ direction. The number of ions detected $N(\psi)$ was stored in a computer memory in circa 1000 channels. The measuring time per distribution was 100 sec.

The number of detected ions per channel showed only the statistical spread (the square root of the number of detected ions), which was 3% on the average for the measured points contained in the results shown in section 4.

The resulting azimuthal distributions measured in this way in different experimental circumstances are shown in the next section as continuous curves (smoothed manually) without error indication.

4. Experimental and calculated results for Ne^+ ion scattering

4.1. Scattering by Cu on clean Cu(1̄10)

A clean Cu(1̄10) surface (oxygen coverage <1% of the saturation coverage) was used for Ne^+ ion scattering experiments on the Cu surface atoms. In fig. 5 the azimuthal distributions for 5 keV Ne^+ ions (current density 4 $\mu A/cm^2$ perpendicular to

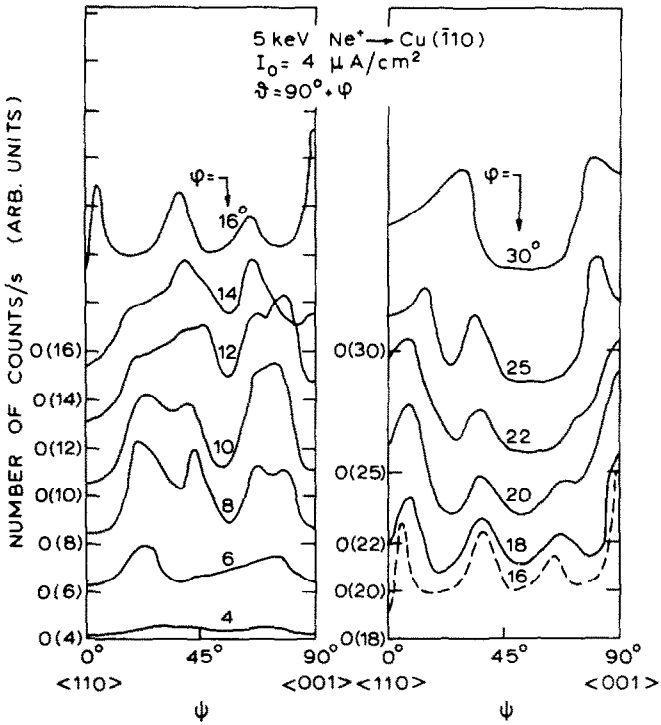

Fig. 5. Measured yield of Ne^+ ions scattered by Cu atoms on a clean Cu(1̄10) surface (oxygen-coverage <1% of oxygen saturation coverage) as a function of the azimuthal angle ψ (relative to the ⟨110⟩ direction in the surface) for different angles φ (relative to the surface plane). The curves are separated by a vertical shift of the origin (O(4), O(6), ...).

the primary beam direction) scattered by Cu atoms are shown at different angles of incidence φ. The detection direction was normal to the target surface. When the projection of the direction of the incoming Ne^+ ions incident on the target surface is along close-packed directions in the surface plane, such as ⟨110⟩, ⟨112⟩ and ⟨001⟩, corresponding with $\psi = 0°$, 55° and 90° respectively, dips are found for small angles of incidence ($\varphi < 15°$). For larger angles of incidence ($\varphi > 15°$) peaks appear for some of these azimuthal directions (e.g. $\varphi = 16°$ and $\psi = 90°$). At still higher angles of incidence φ these peaks disappear again leaving only a dip in the ⟨112⟩ direction at $\psi = 55°$. Minor differences in the measured positions of peaks were found when different Cu(1̄10) crystals were used.

The behaviour of all these curves can be explained with the help of the shadow cone model mentioned earlier. The intensities as a function of φ and ψ are directly related to the position of atoms which lie next to a certain Cu atom on the surface, namely *inside* the shadow cone, *at* the edge of that shadow or *outside* the shadow cone of that particular Cu atom.

Looking at the model of a Cu(1̄10) surface (fig. 6), one can imagine that at very low angles of incidence φ the atoms A, B and C are inside the shadow cone of atom *M* (depending on ψ). This means that in the ⟨110⟩ direction, for example, hard single collisions at Cu atoms are impossible because all the atoms are lying in each other's shadow cones. The same remarks apply to the ⟨001⟩ and the ⟨112⟩

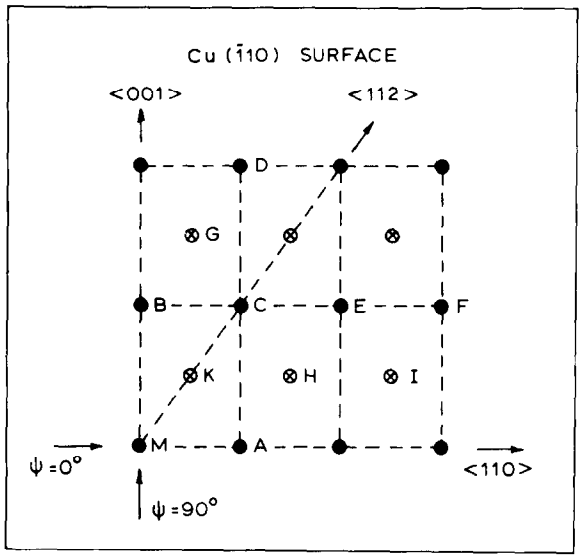

Fig. 6. Schematic presentation of the first two layers of a Cu(1̄10) surface: (•) Cu atoms in the surface plane; (⊗) Cu atoms in the second layer (1.3 Å below the surface plane).

directions. However, when one increases φ at $\psi = 90°$, then at a certain value atom B suddenly comes into the area at the edge of the shadow cone and a strong collision with this atom becomes possible. Such collisions will produce a large quantity of reflected ions (see fig. 5, at $\varphi = 16°, 18°, 20°$, $\psi = 90°$). The same remarks apply to the ⟨110⟩ direction ($\psi = 0°$), but at still higher angles of φ (e.g. $\varphi = 18°$). If φ is larger than 18° a hard collision is possible at all surface atoms. At angles greater than $\varphi \approx 20$–$22°$, only focussing effects on the second layer (on atoms lying at the edge of one or more shadow cones) and channelling effects play a part. The latter effects are seen for instance at $\psi = 55°$ and $\varphi = 30°$. In this direction there are indeed ⟨011⟩ channels in the crystal.

A quantification of these explanations is found in the results of computer calculations given in fig. 7. The calculated scattering yield is plotted versus the azi-

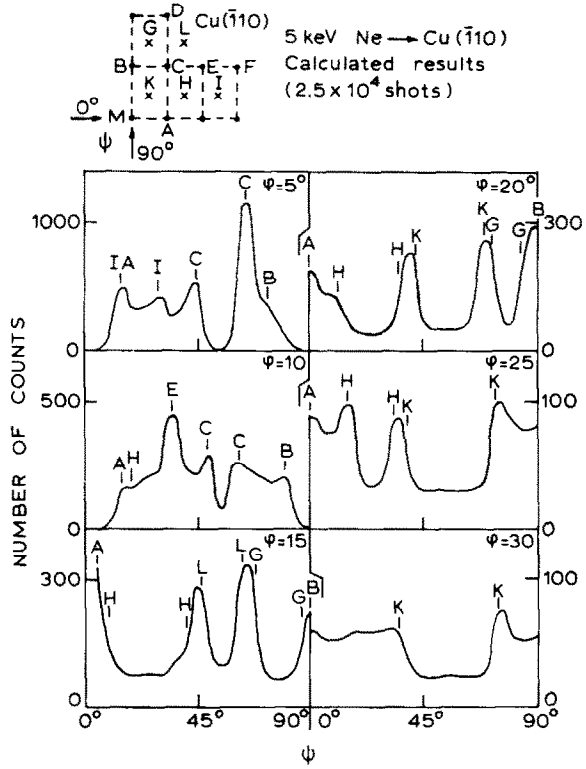

Fig. 7. Calculated scattering yields of 5 keV Ne particles scattered by Cu atoms in a Cu(1̄10) surface (firstly by *M* and then by A, B, C, etc.). The yields are given as a function of azimuthal angle for different angles of incidence φ as indicated. The peaks are marked with the corresponding letter of the atom where an enlarged flux of Ne atoms is found due to the shadow cone of atom *M*.

muthal angle ψ at different elevation angles of incidence φ. In fig. 7 the origin of the different peaks is indicated by a letter that corresponds to a neighbouring atom where an enlarged flux of Ne particles has been found due to atom M. The calculations were performed using an inverse square power interaction potential (ar^{-2} with $a = 132$ Å^2 eV) between a Ne atom and a Cu atom. Bombardment of the surface with a homogeneous ion beam was imitated by the calculations. At certain angles ϕ and ψ many different impact points of the primary particle were chosen within a unit surface cell (around atom M lying in the centre of a crystal surface). The scattering angles were calculated for successive binary collisions between the incident Ne atom and the target atoms of the first two surface layers. The scattering yield was calculated by counting the number of particles scattered within a certain space-angle interval and energy interval (analogous to the experimental circumstances). The calculated results can be compared only qualitatively with the experimental results (i.e. position of peaks and dips and not magnitudes), because neutralization effects are not taken into account.

The correspondence between measured (fig. 5) and calculated (fig. 7) peaks and dips shows the applicability of the shadow cone model for these experiments. Small differences between the measured and calculated position of the peaks are attributed to the selective detection of the ionized particles and to the somewhat arbitrarily assumed interaction potential between the incoming atom (ion) and the surface atom.

4.2. Scattering by Cu on oxygen-covered Cu($\bar{1}10$)

The experiments on oxygen-covered Cu($\bar{1}10$) surfaces were performed by means of Ne^+ ion scattering measurements at an oxygen pressure of 10^{-6} Torr in the target chamber. At this oxygen pressure the oxygen coverage varied between 90% and 100% of the saturation coverage for all angles of incidence and at the ion intensities used [5]. According to a recent AES–LEED–ellipsometry study [3] the saturation coverage is about half a monolayer.

Fig. 8 shows the azimuthal distributions for 4 keV Ne^+ ions scattered by the Cu atoms. Comparison with results for a clean Cu($\bar{1}10$) surface (curve a) shows that the overall structure of the distributions is almost equal. The only difference is that there is an extra peak near the ⟨110⟩ direction. This behaviour was also found at other elevation angles φ smaller than 13°. The extra peak disappears at larger φ values. There is therefore good reason to assume that this peak is due to the shadow cone of the oxygen.

This overall correspondence between the azimuthal distributions from clean and from oxygen-covered Cu($\bar{1}10$) surfaces leads us to conclude that the displacements of the copper atoms in and perpendicular to the surface plane of an oxygen-exposed Cu($\bar{1}10$) surface at room temperature are less than 4% of the interatomic distances (2.56 Å).

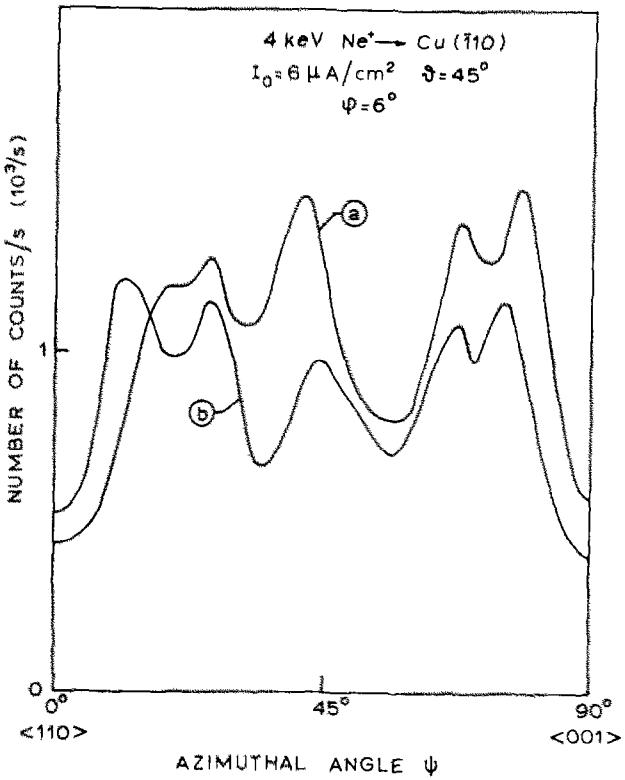

Fig. 8. Measured yield of Ne^+ ions scattered by Cu atoms on a Cu(1̄10) surface partially covered with oxygen as a function of the azimuthal direction (curve b). The results are compared with those on clean Cu (curve a).

4.3. Scattering by O on oxygen-covered Cu(1̄10)

The experimental conditions (e.g. oxygen pressure and coverage) were the same as in section 4.2. Again the peaks and dips in the distributions shown in fig. 9 depend on the azimuthal angle ψ and elevation angle of incidence φ. An estimate of the oxygen position on the Cu(1̄10) surface can be made before a detailed explanation of these experimental results is given.

At very small angles of incidence φ (e.g. $\varphi = 3°$) appreciable scattering is found only near the ⟨110⟩ direction. At larger values of φ we find hardly any oxygen scattering at $\psi = 0°$. This means that the oxygen atom is always in the shadow cone of a Cu atom in the ⟨001⟩ chain for φ values smaller than 15°.

Therefore we can conclude that the oxygen atoms are situated in a ⟨001⟩ surface chain, or to be more precise in a (110) plane normal to the surface. Since the oxygen was always found in the ⟨110⟩ direction and the azimuthal distributions were

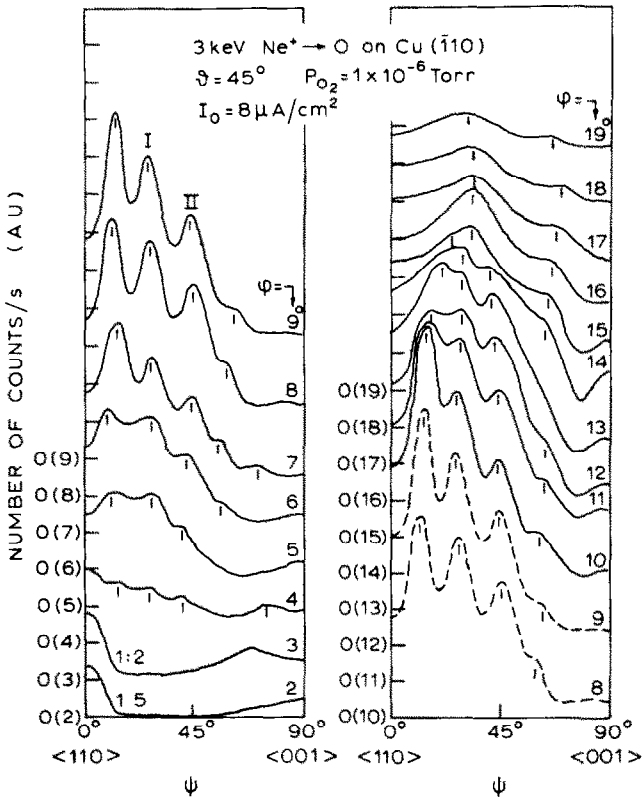

Fig. 9. Measured yields of the Ne^+ ions scattered by O atoms chemisorbed on a CU(1̄10) surface as a function of the azimuthal angle ψ for different elevation angles of incidence φ as indicated ($\varphi = 2°, 3°, ...$). The curves are separated by a vertical shift of the origin (O(2), O(3), ...).

symmetric around this ⟨110⟩ direction (which was measured but not shown in the figures), it is reasonable to assume that the position of the oxygen is at the same distance from two neighbouring Cu atoms in this ⟨001⟩ chain. Knowing this aspect of the position of the oxygen on the Cu(1̄10) surface we can expect that in a ⟨111⟩ direction ($\psi = 35°$) the distributions will behave in accordance with this position. This means that the oxygen atom will sometimes be in the shadow cone of atom B of fig. 10a.

We do indeed see a peak on each side of this incidence direction ($\psi = 35°$) at $\varphi =$ 6–14°. These two peaks (in fig. 9 indicated by I and II) can be explained by the shadow cone model. The two peaks are formed because in these azimuthal directions the oxygen atom is at the edge of the shadow cone of atom B. In fig. 10b the position of these two peaks (and also the position of other peaks) represented by

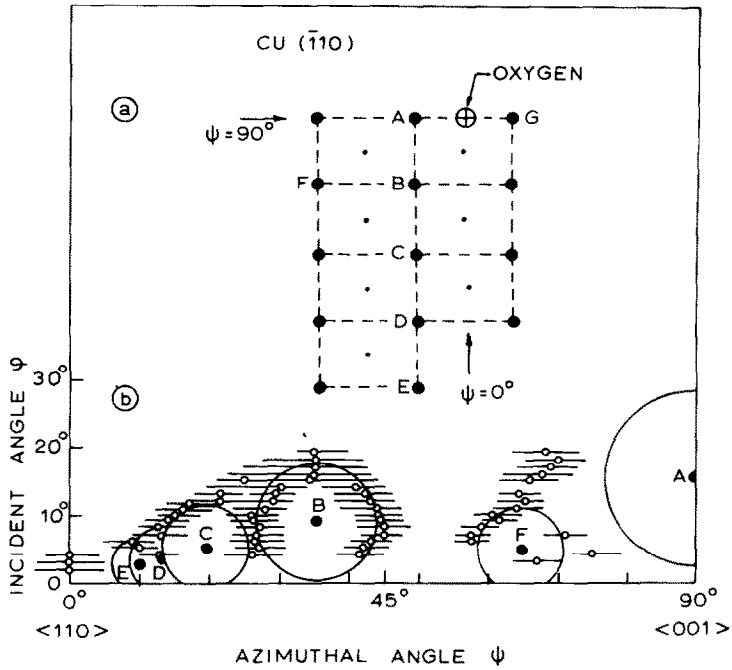

Fig. 10. (a) Schematic drawing of the Cu(1̄10) surface plane, with a projected O atom between two next nearest neighbour Cu atoms. (b) Peak positions (as deduced from fig. 9) shown in $\varphi-\psi$ diagram and given by small circles with bars indicating the peak widths. The large circles correspond to undisturbed shadow cones belonging to the indicated Cu atoms (see text).

small circles with bars indicating the peak width, are shown in a $\varphi-\psi$ plot for the different angular distributions of fig. 9.

From fig. 10b it follows that the largest angle between the two scattering maxima around $\psi = 35°$ is found at $\varphi = 9°$. This means that at these angles of incidence φ and ψ the oxygen atom is right in the middle of the shadow cone of atom B.

Knowing the values of φ and ψ and the distances between surface atoms (2.56 Å and $2.56\sqrt{2}$ Å), we can now calculate the position of the oxygen below the surface layer. The value for the impact parameter, which causes a scattering angle of 45° for Ne^+ on O, can be estimated as 0.1 Å for different types of interaction potentials between Ne and O (for the used primary energy of 3 keV). The impact area of the oxygen atom is found to be 0.5 ± 0.1 Å below the surface plane. So the distance of the oxygen atom centre to the surface plane is approximately 0.6 ± 0.1 Å.

Starting with this calculated position, one may expect that at $\psi = 35°$ and $\varphi = 9° + \frac{1}{2} \times 18°$ (the value of 18° is the estimated value for the largest angle between the two scattering maxima around $\psi = 35°$ at $\varphi = 9°$) the oxygen atom will be at the edge of the shadow cone of atom B. A peak is indeed seen when φ is equal to

this value ($\varphi = 18°$). However, this peak is also visible for $\varphi = 16°$ and $\varphi = 17°$. It should be pointed out that thermal vibrations of the surface atoms normal to the surface plane can cause this spread in φ. So we can conclude that our estimate of the oxygen atom position is correct. A more detailed discussion of the experimental results given in fig. 9 is necessary to explain the background of Ne^+ ions scattered by oxygen in directions where total shadowing takes place. The background signal is partly caused by a broadening of the peaks in the distributions due to the angular resolution of the analyzer system ($\Delta\varphi = 3.5°$ and $\Delta\vartheta = 6.5°$) and the angular spread of the primary beam (1°). Thermal vibrations of the Cu and O atoms in the target surface also give rise to peak broadening. These effects, however, cannot explain the background in the ⟨001⟩ direction (see e.g. the distribution for $\varphi = 9°$ or 10° in fig. 9). The most important contribution to the background is supposed to be supplied by ions scattered from deeper layers. (This supposition will be discussed in more detail in section 5). Scattering by physisorbed oxygen or oxygen in the vicinity of surface defects may also contribute to the background signal.

The calculated position of the oxygen is used to calculate the φ and ψ values at which the oxygen atom lies at the edge of a shadow cone of a certain Cu atom. The results are circles in a φ–ψ diagram. This is demonstrated in fig. 10b for different atoms indicated by A, ..., F. The disturbance of the shadow cones by neighbouring atoms is neglected in the calculations. If the influence of neighbouring atoms is taken into account, the given circles will be somewhat distorted. This distortion will be small, if the distance between a neighbouring atom and the edge of a shadow cone is relatively large (see for instance fig. 1, where for $P \geqslant 0.7$ Å the particle is only slightly deflected). This situation is valid for atoms A, B and F (see fig. 10b). The intensity of the peak at C and D (see fig. 9, e.g. at $\varphi = 9°$, $\psi = 13°$) suggests that the combined shadow cones of atom C and D give a large flux of particles on the oxygen atom. This is the so-called ion focussing or wedge focussing effect [25–27]. The combined effects of the shadow cones of atom C and B also give rise to a high intensity (indicated by I in fig. 9). No peaks are found for atom A because of blocking effects by atom G; Taking these considerations into account, the overall agreement between the calculated and experimental results is remarkably good (see fig. 10).

5. Final remarks and conclusion

The measured angular distributions of scattered ions $N(\psi)$ show a large number of peaks and dips. The used primary energy range (3–5 keV) is an optimum for the appearance of structure in the measured distribution on the one hand and the interpretation of the structure on the other hand. With low primary ion energies less structure is visible in the distributions, probably because of neutralization effects. High primary ion energies increase the influence of deeper layers in the measured distributions and complicate the interpretation of the origin of peaks and dips. The

best way of interpreting the presented distributions is to start with the large dips, which always originate from close-packed directions. The interpretation of the origin of peaks in the ψ distributions is sometimes complicated by the fact that the positions of the peaks may be shifted by simultaneous interaction of neighbouring Cu atoms on the scattered Ne^+ ions. Moreover two or more neighbouring atoms can give rise to a peak at a non-trivial place in the distribution.

Nevertheless the peaks in the distributions, originating from the enlarged flux at the edge of a shadow cone, are useful to determine positions of adsorbed atoms on a surface, as we found in the case of oxygen on a Cu($\bar{1}10$) surface.

The measurement of angular distributions of scattered ions is a direct method for determining adsorbed-atom positions above and below the surface plane. In the special case studied here, Ne^+ ions scattered by oxygen, only scattering angles below 53° are possible according to the single collision model. This means that Ne^+ ions scattered on oxygen atoms below a Cu surface layer might be blocked by surface atoms after being scattered on the oxygen. This blocking effect can also cause a dip in the angular distribution at certain angles of incidence and certain scattering angles. The blocking effects possibly influence the measured distributions of Ne^+ ions scattered by oxygen on a Cu($\bar{1}10$) surface in the $\langle 110 \rangle$ direction (see figs. 9 and 10, where there are no peaks near atom A).

The explanation given for the experimental results was justified in the case of a clean Cu surface, because of the agreement between the calculated and measured distributions.

This agreement was not only in the positions of the peaks and dips but also in the elevated background for $\varphi = 16^\circ - 30^\circ$ (see figs. 5 and 7). The explanations for this background is that scattering by all surface atoms is possible at these elevation angles of incidence. The absence of background at smaller elevation angles (in calculated and in experimental distributions) indicates the absence of surface defects (adatoms and surface steps).

In the case of oxygen on a Cu($\bar{1}10$) surface, similar calculations are necessary to explain all the details in the measured angular distributions. These calculations are not essential for the determination of the position of the oxygen on the Cu surface as has been shown already. No comparisons of the determined oxygen position on Cu($\bar{1}10$) are possible because no experimental data are available (as far as the authors know) except LEED data [6–8], which gives a (2×1) structure in the case of oxygen on Cu($\bar{1}10$). Comparisons with LEED data are complicated because LEED experiments are generally performed with the adsorbed layer in a static situation, whereas our results are obtained in a dynamical situation, i.e. oxygen was admitted during bombardment. The oxygen coverage degree results from an equilibrium between the number of adsorbed oxygen particles and the number of desorbed and sputtered oxygen particles. Although ion bombardment may influence the measured oxygen position in the first surface layer, control measurements in a static situation did not indicate any such influence.

With regard to the experiments on oxygen-covered Cu surfaces another remark

should be made. In measured energy spectra of Ne^+ ions on oxygen-covered Cu($\bar{1}10$) surfaces (i.e. fig. 4b) an increased number of counts was measured on the low energy side of the Ne^+–Cu scattering peak. This increased number of counts was also measured for incidence directions in which hardly any oxygen scattering was observed in the energy spectra (e.g. at $\psi = 90°$, where the oxygen atom is inside the shadow cone of a Cu surface atom). Such behaviour was found on Cu(111) too. On clean copper surface this low energy tail in the energy spectra of Ne^+ ions is absent for the used primary ion energies. The increased number of counts at the low energy side of scattering peaks can be attributed to particles which followed rather complicated trajectories in or below the surface layer and most of them have therefore been neutralized. Since the increased tail in the energy spectra for oxygen-covered surfaces can not originate from multiple scattering from oxygen rows or Cu–O rows, this probably means that the oxygen on the surface causes an enlarged ionization probability or a decreased neutralization probability for Ne particles scattered below or in the uppermost surface layer. This tail can be used for studying the neutralization of scattered particles or for investigating second surface layers.

To conclude, low energy ion scattering experiments are a useful tool for investigating adsorbed layers. In those cases where the adsorbed atoms are in regular positions above or below the crystal surface, the low energy of the incoming ions makes it possible to determine the relative position of the adsorbed atoms with the help of the shadow cone model.

Acknowledgement

This work is part of the research programme of the Foundation for Fundamental Research on Matter (FOM) and was financially supported by the Netherlands Organization for the Advancement of Pure Research (ZWO).

References

[1] See for example: A.W. Czanderna, Ed., Methods of Surface Analysis (Elsevier, Amsterdam, 1975).
[2] F.H.P.M. Habraken, E.P. Kieffer and G.A. Bootsma, in: Proc. 7th IVC and 3rd ICSS (Vienna, 1977) p. 877.
[3] F.H.P.M. Habraken and G.A. Bootsma, Ned. Tijdschr. Vacuum Tech. 16 (1978) 142 (ECOSS I, Amsterdam, 1978).
[4] E. Taglauer, G. Marin and W. Heiland, Appl. Phys. 13 (1977) 47.
[5] A.G.J. de Wit and J.M. Fluit, to be published.
[6] G. Ertl, Surface Sci. 6 (1967) 208.
[7] G.W. Simmons, D.F. Mitchell and K.R. Lawless, Surface Sci. 8 (1967) 130.
[8] A. Oustry, L. Lafourcade and A. Escaut, Surface Sci. 40 (1973) 545.

[9] W. Heiland, F. Iberl, E. Taglauer and D. Menzel, Surface Sci. 53 (1975) 383.
[10] Yu.V. Martynenko, Soviet Phys. Solid State 6 (1965) 1581.
[11] Yu.V. Martynenko, Radiation Effects 20 (1973) 211.
[12] H. Goldstein, Classical Mechanics (Addison-Wesley, Reading, MA, 1974) p. 58.
[13] G. Leibfried, Bestrahlungseffekte in Festkörpern (Teubner, Stuttgart, 1965) p. 30.
[14] P.B. Firsov, Soviet Phys. JETP 5 (1957) 1192; 6 (1958) 534; 7 (1958) 308.
[15] A.A. Abrahamson, Phys. Rev. 130 (1963) 693.
[16] A.A. Abrahamson, Phys. Rev. 178 (1969) 76.
[17] D.P. Smith, J. Appl. Phys. 38 (1967) 340.
[18] W. Heiland and E. Taglauer, J. Vacuum Sci. Technol. 9 (1972) 620.
[19] H.H. Brongersma and P.M. Mul, Surface Sci. 35 (1973) 381.
[20] H.H. Brongersma and J.B. Theeten, Surface Sci. 54 (1976) 519.
[21] E.S. Mashkova, V.A. Molchanov and Yu. G. Skripka, Dokl. Acad. Nauk 198 (1971) 809.
[22] W.C. Turkenburg, W. Soszka, F.W. Saris, H.H. Kersten and B.G. Colenbrander, Nucl. Instr. Methods 132 (1976) 587.
[23] W. Heiland, H.G. Schäffler and E. Taglauer, Surface Sci. 35 (1973) 381.
[24] A.G.J. de Wit, G.A. van der Schootbrugge and J.M. Fluit, Surface Sci. 47 (1975) 258.
[25] E.S. Mashkova and V.A. Molchanov, Radiation Effects 19 (1973) 29.
[26] E.S. Mashkova and V.A. Molchanov, Radiation Effects 23 (1974) 215.
[27] H.H.W. Feyen, L.K. Verhey, E.P.Th.M. Suurmeyer and A.L. Boers, in: Proc. 5th Intern. Conf. on Atomic Collisions in Solids (Plenum, New York, 1975) p. 573.